

Four-PAM Modulation of Ambient FM Backscattering for Spectrally Efficient Low-Power Applications

Spyridon Nektarios Daskalakis^{ID}, *Student Member, IEEE*, Ricardo Correia^{ID}, *Graduate Student Member, IEEE*, George Goussetis^{ID}, *Senior Member, IEEE*, Manos M. Tentzeris^{ID}, *Fellow, IEEE*, Nuno Borges Carvalho^{ID}, *Fellow, IEEE*, and Apostolos Georgiadis^{ID}, *Senior Member, IEEE*

Abstract—Ambient backscatter uses radio frequency signals available in the environment (e.g., radio broadcasting, television, or mobile telephony) to transmit data effectively leading to significant energy and cost efficiency increase. This paper presents a novel wireless tag, which for the first time utilizes 4-pulse amplitude modulation technique to modulate the ambient backscattered FM signals in order to send data to a nearby low-cost software defined radio reader. The tag is based on an RF front-end that uses a single transistor controlled by an ultralow-power microcontroller. The microcontroller includes an analog-to-digital converter for sensing and a digital-to-analog converter for RF front-end control. A proof-of-concept prototype is demonstrated in an indoor environment with the low bit rate of 345 b/s and power consumption 27 μ W. It operated using a real FM station at 34.5 km away and the tag-to-reader distance was tested at 1 m. The value of energy spent in this modulator was 78.2 nJ/bit at 345 b/s and 27.7 nJ/bit at 10.2 kb/s.

Index Terms—Ambient backscattering, backscatter communication, FM modulation, Internet-of-Things (IoT), pulse amplitude modulation (PAM), radio frequency identification (RFID) sensors, software-defined radio (SDR).

Manuscript received July 6, 2018; revised October 11, 2018; accepted October 24, 2018. Date of publication November 14, 2018; date of current version December 11, 2018. This work was supported in part by the Lloyd's Register Foundation and in part by the International Consortium in Nanotechnology. This work of R. Correia and N. Borges Carvalho was supported in part by the European Regional Development Fund, through the Competitiveness and Internationalization Operational Programme 2020 of the Portugal 2020 framework, Project, MOBIWISE, POCI-01-0145-FEDER-016426 and in part by FCT/MEC through national funds and when applicable co-funded by the FEDER PT2020 partnership agreement under Project UID/EEA/50008/2013. The work of M. M. Tentzeris was supported in part by the National Science Foundation and in part by the Defense Threat Reduction Agency. This paper is an expanded version from the 2018 IEEE MTT-S International Microwave Symposium 2018, Philadelphia, PA, USA, June 10–15, 2018. (*Corresponding author: Spyridon Nektarios Daskalakis.*)

S. N. Daskalakis, G. Goussetis, and A. Georgiadis are with the School of Engineering and Physical Sciences, Institute of Sensors, Signals and Systems, Heriot-Watt University, Edinburgh, EH14 4AS, U.K. (e-mail: sd70@hw.ac.uk; g.goussetis@hw.ac.uk; apostolos.georgiadis@ieee.org).

R. Correia and N. Borges Carvalho are with the Departamento de Electrónica, Telecomunicações e Informática, Instituto de Telecomunicações, Universidade de Aveiro, 3810-193 Aveiro, Portugal (e-mail: rjoao@ua.pt; nbcarvalho@ua.pt).

M. M. Tentzeris is with the School of Electrical and Computer Engineering, Georgia Institute of Technology, Atlanta, GA 30332-250 USA (e-mail: etentze@ece.gatech.edu).

Color versions of one or more of the figures in this paper are available online at <http://ieeexplore.ieee.org>.

Digital Object Identifier 10.1109/TMTT.2018.2879105

I. INTRODUCTION

ONE of the key challenges for practical Internet-of-Things and wireless sensor networks is the delivering autonomy to a massive number of devices which conventionally need to be powered with batteries. Moreover, ensuring low cost is an equally important parameter pertaining to the viability of such systems. Low-power and low-complexity backscatter communications have emerged as a promising paradigm to address aforementioned challenges. This technology delivers ultralow-cost and ultralow-power wireless communications by modulating the reflection of incident radio frequency (RF) carrier signals. Due to their advantageous features, backscattering communications have been increasingly exploited in radio frequency identification (RFID) systems [1].

In order to maintain low-cost and power efficient operation, the RF topologies of typical sensor nodes (tags) preferentially involve an antenna and a circuit with a single RF transistor, as for example in [2]. The communication setup can be implemented in a bistatic or monostatic architecture and requires an RF carrier wave (CW) emitter, the tag, and a reader. Traditional batteryless RFID systems utilize monostatic architectures where the reader includes the transmitter (CW emitter) and the receiver. Binary amplitude shift keying (ASK) or phase shift keying (PSK) modulations are commonly used for the communication between the tag and reader, such that information is encoded using two states of the amplitude or the phase of the reflected CW [3]. For example, in the WISP platform [4], the electronic product code (EPC) protocol employs 2-ASK modulation to encode the bits 1 and 0 with long and short gaps in RF power, respectively. Recently, a body implanted device powered by a 13.56 MHz wireless power transfer (WPT) link, uplinks neural data at 915 MHz using a binary PSK (BPSK) backscatter modulation [5]. In the aforementioned examples, the reader provides the CW for supply and communication purposes.

In order to increase the data rate, other works have exploited higher order modulation schemes for semipassive and passive sensor networks [6]–[8]. Thomas *et al.* [7] present a 4-quadrature amplitude modulation (QAM) scheme for backscatter communication enabling the transmission of 2 bits

per symbol instead of 1 bit with two ASK, effectively increasing the data rate and leading to a reduced on-chip power consumption. The modulator involved a battery-assisted (semipassive) and a passive tag operating in the range of 850–950 MHz. This system demonstrated transmission of 4-PSK/4-QAM with a bit rate of 400 kb/s and with static power dissipation of 115 nW. The backscatter modulator uses four lumped impedances connected to an RF switch and it was controlled by a microcontroller. The same authors developed a 16-QAM modulator for ultrahigh-frequency (UHF) backscatter communication with five switches. Using a 16-to-1 multiplexer, they were able to modulate the antenna load between 16 different states [9]. The tag was tested on a 915 MHz, +23 dBm, and CW signal. The tag-to-reader range was measured at 1.24 m with a high bit rate 96 Mb/s. In [10], a novel backscatter modulator is presented which employs a Wilkinson power divider and two switches. The divider introduces a phase shift in one of the branches and two transistors acting as switches. High-order backscatter modulations of M-QAM or M-pulse amplitude modulation (PAM) can be achieved as each transistor can be controlled with different voltage levels to achieve different reflection coefficient values. The 16-QAM modulator demonstrated in [10] features an energy consumption as low as 6.7 pJ/bit for a bit rate of 120 Mb/s. Reference [11] presents a 5.8 GHz RF-powered Si CMOS transceiver with 32-QAM communication scheme. The uplink part uses the backscattering technique with a modulation 32-QAM, while consuming $113 \mu\text{W}$ at 0.6 V. The RF front-end of the design consists of two transistors and the quadrature modulation is realized by two intermediate frequency (IF) signals (I/Q). In [12], a tutorial survey of backscatter modulation is provided as an emerging means for short-range low-rate communications. It provides the relationship between on-tag power harvesting and forward error correction applied to the higher order modulation work [6].

In recent works, existing ambient RF signals have been proposed for backscatter communication instead of a CW emitter signal [13], [14]. This approach simplifies the complexity and cost of the system and its deployment. Reference [13] presents two RF-power devices that communicate between them exploiting the scattering of ambient TV signals. In [15], a backscatter PSK hardware prototype is presented that combines a 4-PSK transmitter, an energy harvester and a multilevel voltage detector. Two similar prototypes can communicate with data rate of 20 kb/s using an ambient signal from UHF TV band. In [16], a dual-band 4-QAM backscatter modulator circuit was proposed for ambient signals. It is composed by two transistors and a dual-band Wilkinson power divider, following the same principle proposed in [10]. The modulator presents an average power consumption of 27 nW for 500 kb/s of data rate at 900 MHz and 2.45 GHz (cellular and Wi-Fi frequencies). In [17], broadcast frequency modulated (FM) signals have been used to power the tag and enable effective communication between tag and reader. The transmitted power of FM signals is higher than AM signals, TV and GSM signals and hence can deliver better communication range between the tag and reader. The initial implementation of [17] was able to communicate over distances of several feet, even in

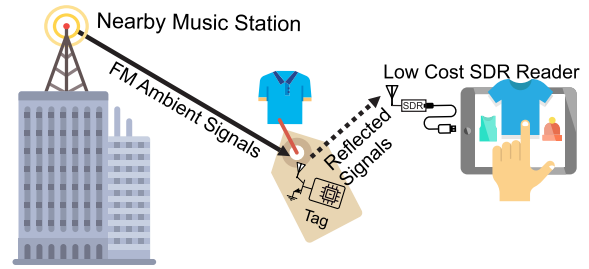


Fig. 1. FM ambient backscatter communication scheme. An example application could be the identification of clothes in a mall using tablets and low cost SDRs.

cases where transmission towers were up to many kilometers away.

Our previous work [18] demonstrated a tag capable of transmitting FM reflections to a computer or a tablet through a low-cost software defined radio (SDR) reader. Fig. 1 depicts a possible application of this system. The tag uses ASK binary modulation with FM0 encoding on ambient FM station signals as in commercial RFID systems. The FM transmitter was 34.5 km away from the measurement's setup and a 5 m communication range between the tag and the reader was achieved with 2.5 kb/s bit rate. A theoretical analysis of the error rate performance also provided [18].

In [17], for the first time, the high-order modulation was introduced for ambient backscattering communications. The authors demonstrated 4 frequency-shift keying (FSK) modulation to transmit 2 bits per symbol over the ambient FM signals with a maximum data rate 3.2 kb/s. The work involves the simulation of an integrated circuit for the tag, while for the prototype an arbitrary waveform generator (AWG) was used connected with an RF front-end.

In this work, we consider high-order amplitude modulation and we demonstrate the first prototype suitable for ambient backscatter communication deployment working with 4-PAM. The FM frequencies were selected due to the strong ambient signal source that can be used for backscatter communication. The 4-PAM modulation is used to double the bit rate, compared to a 2-PAM system. With amplitude modulation, the complexity of the receiver and the tag can be drastically simplified as there is no need for a different frequency for each symbol. Tag and receiver are more complex as variation of modulating signal has to be converted and detected from corresponding variation in frequencies. Preliminary results were presented in previous work [19], where 4-PAM scheme was selected due the low hardware complexity and low-power consumption. This work is an extensive presentation of the FM backscatter system in [19], thus the theoretical analysis of the system is provided as well as a real-time receiver implementation. Additional details about the tag are also provided. In particular, our tag employs a single low cost transistor and a telescopic antenna achieving communication with low bit rate for reduces power consumption. This work differs from [9] and [10] since it uses ambient FM signals as the carrier instead of an intentionally transmitted unmodulated CW signal. The use of FM signals on the receiver increases

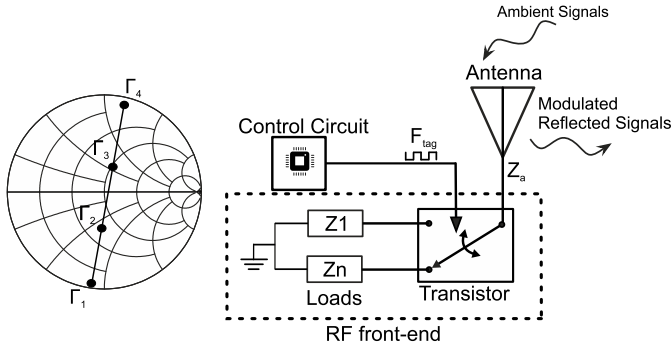


Fig. 2. Backscatter radio principle: an RF transistor alternates the termination loads Z_i of the antenna corresponding to different reflection coefficients Γ_i . Four reflection coefficients ($n = 4$) could create a 4-PAM.

the complexity of selecting the thresholds associated with demodulation, as explained below in Section V. In particular, we present a tag consisting of a microcontroller (MCU) with a digital-to-analog converter (DAC) and an analog-to-digital converter (ADC). The tag could collect data from sensors through the ADC and process them. The MCU creates the modulation pulses internally and controls the RF front-end transistor via the DAC. A low cost SDR receiver is used similar to [18].

This paper is structured as follows. Section II reviews the principles of the proposed backscatter communication systems. Section III describes the tag hardware implementation. Section IV provides the theory and performance analysis of the FM ambient 4-PAM technique. Section V discusses the theory, as well as the hardware and software elements of the receiver. In Section VI, the proof-of-concept experimental communication results are presented. Section VII provides the comparison of our work with other similar high-order modulation works. Finally, Section VIII concludes this paper.

II. BACKSCATTER MODULATION

In backscatter communications, the tags do not need to transmit a radio signal, since they reflect signals transmitted by the reader or another ambient radio emitter. A backscattering tag modulates the reflected signal using one or more transistors or RF switches connected to the antenna as it is shown in Fig. 2. A binary backscatter communication is based on a reflected waveform that should switch between a fully matched and a short circuit load terminating the antenna. In [18], an RF switch was directly connected to the RF front-end antenna in order to create the two discrete states. For high-order modulations, the number of states has to be increased and the RF circuit must create a specific discrete impedance for each transmitted symbol. For this purpose, a single RF transistor circuit can be used as an active load in order to create different impedances for the PAM constellation [10]. In this work, an E-pHEMT transistor was used to implement a circuit compatible with a 4-PAM scheme. The RF circuit presents four distinct impedance values for a four different gate voltages. A given antenna with impedance Z_a connected to a complex load with impedance $Z_i \in \{Z_1, Z_2, Z_3, Z_4\}$, is associated with

TABLE I
FOUR-PAM MODULATION PARAMETERS

Γ_i	Symbol	Bits	V_{gate} (mV)
$-0.7245 - j0.6922$	-3	00	0
$-0.3414 - j0.2881$	-1	01	333
$+0.0223 + j0.1779$	+1	11	387
$+0.3079 + j0.6334$	+3	10	600

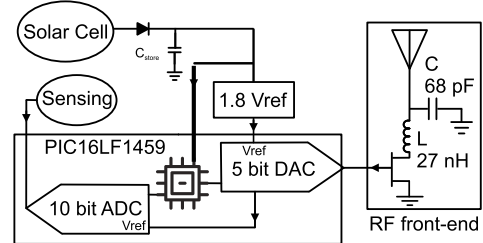


Fig. 3. Schematic of proof-of-concept tag. A low-power micro-controller reads the sensors and controls the RF front-end circuit.

a reflection coefficient obtained as

$$\Gamma_i = \frac{Z_i - Z_a^*}{Z_i + Z_a} \tag{1}$$

Typically, the antenna impedance is chosen to be 50Ω . By changing the gate voltage of the transistor, four distinct reflection coefficients can be achieved corresponding to the four symbols. The performance of PAM modulation is optimized when the Γ_i values lie equidistantly along a straight line on the Smith chart [Fig. 2 (left)] [10]. Considering the above, we can select the desired values of the reflection coefficients; an example of four equidistant measured values on the same line is shown in Table I. Using Table I and (1), the desired voltage values at the transistor gate can be obtained.

The received signal can be expressed in the following complex baseband form [18]:

$$y_r(t) = [\alpha_{dc} e^{j\phi_{dc}} + \alpha_{mod} e^{j\phi_{mod}} \Gamma_i(t - \tau)] e^{-j2\pi \Delta F t} + n(t) \tag{2}$$

with $\alpha_{dc}, \alpha_{mod} \in \mathbb{R}$, and $e^{j\phi_{dc}}, e^{j\phi_{mod}} \in [0, 2\pi)$. The term $\alpha_{dc} e^{j\phi_{dc}}$ defines the dc component associated with the transmitter broadcast baseband signal. The term $\alpha_{mod} e^{j\phi_{mod}}$ describes the scaling and rotation of the modulated part of the received tag signal. This component depends on a number of factors, including the transmitter signal power, the channel characteristics associated with the links between the transmitter-to-tag and tag-to-reader and the backscattering efficiency of the tag. The term ΔF represents the carrier frequency offset (CFO) between the transmitter (FM station) and the reader. The term $n(t)$ is the complex thermal Gaussian noise at the receiver and the time constant τ depends on the tag-to-reader channel propagation characteristics. The tag signal is a function of Γ_i over time.

III. SENSOR NODE/TAG DESIGN

Our tag consists of an ultralow-power MCU connected with an RF front-end as it is depicted in the block diagram of Fig. 3. The 8-bit PIC16LF1459 MCU from Microchip Inc. was

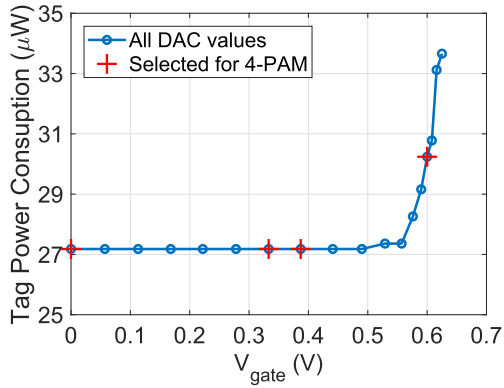


Fig. 4. Digital-to-analog converter output voltage versus the tag power consumption. The tag was measured at 1.8 V when the ADC was turned OFF. Four optimal values were selected for the backscatter communication.

used, which consumes $25 \mu\text{A}/\text{MHz}$ of current at 1.8 V [20]. The clock of the MCU was programmed at 32 kHz in order to minimize the power consumption of the tag. The MCU also has a sleep mode operation with current consumption of $0.6 \mu\text{A}$. The MCU includes a 10 bit ADC and collects data from analog sensors on the tag. The 5-bit DAC of the MCU is used in our application to drive the RF front-end transistor with different voltages. The DAC has the ability to supply the gate of the transistor with 32 distinct voltage levels in order to change the antenna load impedance. Fig. 4 depicts the tag power consumption for all the possible DAC output voltages when the MCU was supplied by a 1.8 V voltage source. Fig. 4 shows the voltages up to 0.625 V, since the maximum voltage for the transistor (DAC output), in our application was 0.6 V. Four DAC outputs were selected for our backscatter modulation scheme as it is explained in more details below. The tag was powered by the flexible solar panel, SP3-37 provided by PowerFilm Inc. [21]. The solar panel charges a $220 \mu\text{F}$ tantalum capacitor instead of a battery through a low-voltage-drop Schottky diode. An external voltage reference IC XC6504 [22] was also used to supply the tag with a stable voltage (V_{ref}) 1.8 V. The proposed sensor node does not focus on a specific sensing application or power management system but only on the novel telecommunication part of the system. An RF harvester could be designed in the future [23] to charge the capacitor during the night in combination with solar cell during the day [24]. Another idea is an integrated cooperative harvester capable of collecting both electromagnetic and kinetic energy simultaneously as proposed in [25].

The RF front-end consists of the ATF52189 E-pHEMT RF transistor from Broadcom [26] and the SRH788 monopole antenna. The maximization of the magnitude of complex reflection coefficient differences between the four states is a main objective for optimized backscatter communication [27]. In this work, a core RF circuit challenge was to achieve the desired change of the drain impedance by varying the voltage at the gate in the range between 0 and 0.6 V. The advanced design system (ADS) from Keysight was used for the optimization of the RF front-end circuit. The simulations

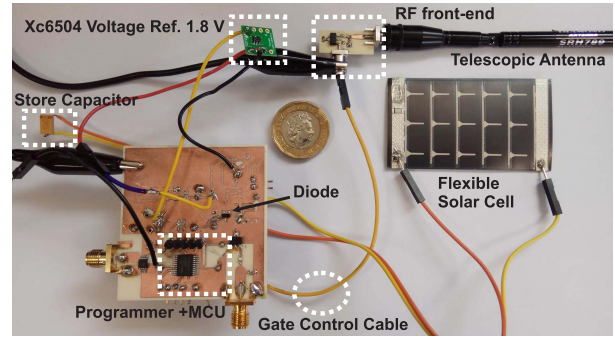


Fig. 5. Fabricated tag prototype with the RF front-end board. The tags are powered by a solar panel.

performed involved the variation of the gate voltage at the transistor from 0 to 0.6 V with a sweep of 0.01 V from 87.5 to 108 MHz. More specifically, the large-signal S-parameter simulation was used to perform the backscatter modulation in order to maximize the distance between the consecutive Γ_i values. Following the aforementioned optimization procedure, the matching network between the transistor and the antenna was composed by a capacitor and an inductor as depicted in the schematic of Fig. 3. In the simulation, we assumed that we have a ideal 50Ω antenna connected with our RF front-end and the optimum component values were found to be 68 pF and 27 nH.

The RF front-end board was fabricated on Astra MT77 substrate with thickness 0.762 mm, $\epsilon_r = 3.0$, and $\tan \delta = 0.0017$. The main board of the proof-of-concept tag that integrates the MCU was fabricated on a Rogers RO4350B substrate. The fabricated prototypes and the solar panel are shown in Fig. 5. As mentioned, the output of the DAC was connected with the gate of the transistor on the RF front-end. The fabricated RF front-end board was measured using a vector network analyzer (VNA) with $P_{\text{in}} = -20 \text{ dBm}$ at the frequencies of the FM band, 87.5–108 MHz. Each DAC output corresponds to a specific reflection coefficient Γ_i and all the possible voltages of Fig. 4 were tested through the VNA. Four voltages: 0, 333, 387, and 600 mV were found as the optimum values to supply the gate of the transistor and create the 4-PAM modulation. The selected values are also depicted in Fig. 4 creating four impedances or symbols for a specific frequency. The measured Γ_i using the four voltages in the FM band are presented in Fig. 6. As it is observed, the selected voltage values offer almost equal distances between the corresponding Γ_i . The prototype board was also tested at -10 and -30 dBm and were exported the same results with Fig. 6. Table I also shows the resulting Γ_i in combination with the symbols, the bits and the gate voltages at a fixed frequency of 95.8 MHz. Using the four voltages at the gate of the transistor and sweeping the frequency, it is possible to observe that each state corresponds to an “arc” on the Smith chart. In particular, the set of four states (each line in Fig. 6) rotates clockwise as the frequency increases. As per the design target, equal distances between the symbols were achieved assuming antenna input impedance equal with 50Ω , in order to maximize the signal-to-noise ratio (SNR) and thus the efficiency of the PAM modulation.

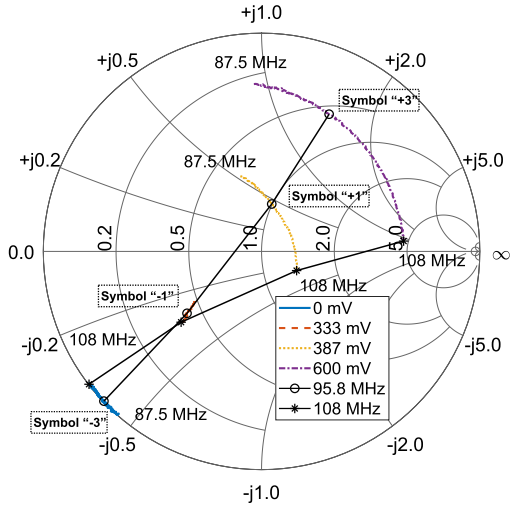


Fig. 6. Smith chart with measured reflection coefficient values for four different voltage levels at the gate of transistor. The pin was fixed at -20 dBm for frequencies 87.5–108 MHz.

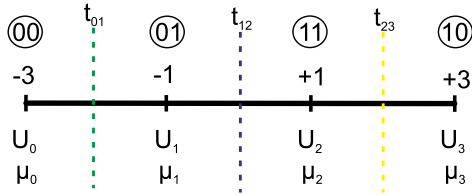


Fig. 7. 4-PAM symbols. Three thresholds are calculated for the decision.

It is noted that our tag is a semipassive design where the available capacitor powers the MCU during transmission from the tag to the reader.

IV. AMBIENT FM 4-PAM MODULATION

PAM is a method of sending information by scaling a pulse shape with the amplitude of the symbols and duration T_{symbol} [28]. In the 4-PAM, there are four symbols and each symbol corresponds to a pair of two bits. Each bit duration is denoted as T_{bit} and the data bit rate is $2/T_{\text{bit}}$ bits per second (b/s). According to 4-PAM, it is possible to transmit two bits with each symbol/pulse, for example, by associating the amplitudes of -3 , -1 , $+1$, and $+3$, with four bit choices 00, 01, 11, and 10 (Table I). The symbols ± 1 and ± 3 are shown in Fig. 7 and the bit representation of the symbols is Gray coded [29]. In order to transmit a digital stream, it must be converted into an analog signal. After conversion of the bits into symbols, the analog form of a 4-PAM modulation signal can be expressed as

$$\Gamma_i(t - \tau) = \sum_{n=0}^{N-1} x_n \Pi[t - nT_{\text{symbol}} - \tau] \quad (3)$$

where $x_n \in \{-3, -1, +1, +3\}$, N is the number of transmitted symbols and $\Pi(t)$ is a pulse with duration T_{symbol} . Thus, each member of the 4-PAM data sequence is multiplied by a pulse that is nonzero over the appropriate time window.

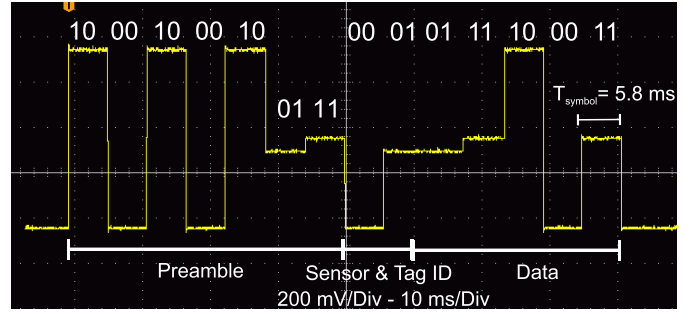


Fig. 8. Oscilloscope measurement of the sending packet. Voltage levels correspond to the four-PAM symbols at the gate of the transistor are presented.

The proof-of-concept tag was set up to send a fixed bit-stream packet format. In this paper, the fixed bit sequence was: 10001000100111–00–01–0111100011 which is translated to symbol sequence: $+3-3+3-3+3-1+1-3-1-1+1+3-3+1$. Transmission of some known preamble data is required at the receiver to identify the beginning of a frame (packet) at the transmission. Here, the first seven symbols (14 bits) were added before the message sequence as a preamble. The symbols of the preamble are used also as training symbols as explained below. After the preamble, “tag number” bits (2 bits), “sensor number” bits (2 bits), and “sensor data” bits (10 bits) follow. The “tag number” bits were utilized in case that four different tags will be used in a future wireless sensor network. With this allocation, the tag could support up to four sensors and the “sensor ID” part is used to identify the sensor number. The last 10 bits section is used for transmitting the sensor data. An example of the transmitted packet is depicted in Fig. 8 and more bits could be added in order to include extra sensors or tags.

V. RECEIVER

A. Receiver Theory

FM radio stations typically operate in the range of frequencies from 88 to 108 MHz and use frequency modulation in order to transmit the audio signals. The FM signals are described in [18] and are given by the formulations x_{FM} and $m(t)$ of the same work. In our case, an FM modulated signal is used for communication instead of a CW signal and the complex baseband received signal is described by $y_{\text{amp}}(t)$ signal in [18] and contains the rectangular pulses of (3).

According to [18] and [30], we can simplify the received complex signal as

$$y_{\text{amp}}(t) \approx Ae^{-jD}e^{jK}h(t) + n(t) \quad (4)$$

with $h(t) = a_1(t) + a_2(t)b(t)$. The term D describes the frequency offset and the term $n(t)$ corresponds to the white Gaussian noise added at the receiver with $n(t) \sim \mathbb{N}(0, N_w)$. The term $h(t)$ contains the useful data signal, $b(t)$, as well as the effects of the channels (FM station-to-reader and tag-to-reader). In the above formulation we assume that the tag and receiver are very close compared to the FM station distance so e^{jK} represents the common delay of the signal received from the FM station. Initially, a similar procedure as in [18]

is followed at the receiver. The received signal is $y_{\text{amp}}(t)$ and its envelope detector is taken in order to remove the CFO term. The obtained signal as in [18] is

$$Z(t) = A^2|h(t)|^2 + w(t) \quad (5)$$

with $w(t)$ Gaussian process [30]

$$w(t) \sim \mathcal{N}(N_w, N_w^2 + 2A^2N_w|h(t)|^2). \quad (6)$$

The signal $Z(t)$ is correlated with a pulse $q(t) = 1$ for $0 < t \leq T_{\text{symbol}}$ and a synchronization procedure is then applied in order to identify the starting point of the frame. A dc removal is required for the synchronization; since the dc term does not contribute with any information on the transmitted data, it can be ignored in the remaining of the receiver processing. The obtained signal can be expressed as

$$\begin{aligned} U_i &= X_i + V_i \\ &= \int_0^{T_{\text{symbol}}} A^2|h(t)|^2 q(t) dt + \int_0^{T_{\text{symbol}}} w(t) q(t) dt. \end{aligned} \quad (7)$$

Using the 4-PAM modulation, $|h(t)|^2$ can take four values ($h_i(t)$) with $i \in \{1, 2, 3, 4\}$, and thus V_i is a Gaussian process

$$V_i \sim \mathcal{N}(T_{\text{symbol}}N_w, T_{\text{symbol}}^2N_w^2 + 2T_{\text{symbol}}^2A^2N_w|h_i|^2). \quad (8)$$

Using $X_i = T_{\text{symbol}}A^2|h_i|^2$ it is straightforward to show that U_i is a Gaussian process with $U_i \sim \mathcal{N}(\mu_i, \sigma_i^2)$. The mean and variance are analyzed as

$$\mu_i = T_{\text{symbol}}A^2|h_i|^2 + T_{\text{symbol}}N_w \quad (9)$$

$$\sigma_i^2 = T_{\text{symbol}}^2N_w^2 + 2T_{\text{symbol}}^2A^2N_w|h_i|^2. \quad (10)$$

Our system works in noncoherent mode where the algorithm does not perform synchronisation between receiver and transmitter. A noncoherent algorithm does not use phase and frequency estimation techniques that add complexity and rate loss at the receiver [31].

For the symbol detection, the minimum distance (maximum-likelihood) rule is used thus no a priori information on the transmitted symbols is available for our system [29]. The decision boundaries and the transmitted constellation for a given measurement U_i , $i \in \{0, 1, 2, 3\}$ are depicted in Fig. 7. Three decision boundaries t_{01} , t_{12} and t_{23} are located between the subsequent symbols. They quantise the signal values as decisions are taken by comparing them with the thresholds. If the symbol error probability can be defined as P_e we can also evaluate the bit error probability (BER) as

$$P_b = \frac{P_e}{2} = \frac{1}{8} \sum_{i=0}^3 P_{e,i} \quad (11)$$

with $P_{e,i}$ the error probability of each symbol. For example, when the symbol -3 was sent, the probability of error is the probability to decide in the right side of threshold t_{01} (Fig. 7) and it is defined as $P(U > t_{01}|U_0)$. The conditional error probability for each symbol can be calculated and simplified

using Q-function accordingly

$$\begin{aligned} P_{e0} &= P(U > t_{e01}|U_{e0}) \\ &= Q\left(\frac{t_{e01} - \mu_0}{\sigma_{e0}}\right) \\ P_{e1} &= P(U > t_{12}|U_{e1}) + P(U \leq t_{e01}|U_{e1}) \\ &= Q\left(\frac{t_{12} - \mu_{e1}}{\sigma_{e1}}\right) + Q\left(\frac{\mu_{e1} - t_{e01}}{\sigma_{e1}}\right) \\ P_{e2} &= P(U > t_{e23}|U_{e2}) + P(U \leq t_{e12}|U_{e2}) \\ &= Q\left(\frac{t_{e23} - \mu_{e2}}{\sigma_{e2}}\right) + Q\left(\frac{\mu_{e2} - t_{e12}}{\sigma_{e2}}\right) \\ P_{e3} &= P(U \leq t_{e23}|U_{e3}) \\ &= Q\left(\frac{\mu_{e3} - t_{e23}}{\sigma_{e3}}\right) \end{aligned} \quad (12)$$

where $Q(x) = (1/\sqrt{2\pi}) \int_x^\infty e^{-t^2/2} dt$ the Q function. For two adjacent conditional probabilities we can assume that

$$P(U = t_{01}|U_0) = P(U = t_{01}|U_1) \quad (13)$$

which is expressed as

$$\frac{1}{\sigma_0\sqrt{2\pi}} e^{-(t_{01}-\mu_0)^2/2\sigma_0^2} = \frac{1}{\sigma_1\sqrt{2\pi}} e^{-(t_{01}-\mu_1)^2/2\sigma_1^2} \quad (14)$$

thus U_0 and U_1 are Gaussian as it was mentioned before. Using the above equality, the threshold t_{01} can be easily calculated as

$$t_{01} = \frac{\sigma_1^2\mu_0 - \sigma_0^2\mu_1}{\sigma_1^2 - \sigma_0^2} \pm \frac{\sqrt{\sigma_1^2\sigma_0^2[(\mu_1 - \mu_0)^2 + (\sigma_1^2 - \sigma_0^2) \ln \frac{\sigma_1^2}{\sigma_0^2}]}}{\sigma_1^2 - \sigma_0^2}. \quad (15)$$

It is clear that the threshold t_{01} is a function of μ_0 and σ_0 parameters and in practice it depends on time-varying received SNR. It is noticed that since $\mu_0 < t_{01} < \mu_1$ only one of the two above solutions is valid for the detection. Also it can be observed that if $\sigma_0^2 = \sigma_1^2$ the threshold can be simplified as $t_{01} = (\mu_0 + \mu_1)/2$ and it is located in the middle between the two symbols. Following the same derivation, the other two thresholds t_{12} and t_{23} are calculated similarly

$$\begin{aligned} t_{12} &= \frac{\sigma_2^2\mu_1 - \sigma_1^2\mu_2}{\sigma_2^2 - \sigma_1^2} \pm \frac{\sqrt{\sigma_2^2\sigma_1^2[(\mu_2 - \mu_1)^2 + (\sigma_2^2 - \sigma_1^2) \ln \frac{\sigma_2^2}{\sigma_1^2}]}}{\sigma_2^2 - \sigma_1^2} \\ t_{23} &= \frac{\sigma_3^2\mu_2 - \sigma_2^2\mu_3}{\sigma_3^2 - \sigma_2^2} \pm \frac{\sqrt{\sigma_3^2\sigma_2^2[(\mu_3 - \mu_2)^2 + (\sigma_3^2 - \sigma_2^2) \ln \frac{\sigma_3^2}{\sigma_2^2}]}}{\sigma_3^2 - \sigma_2^2}. \end{aligned} \quad (16)$$

Next, a simple estimation approach is proposed for the calculation of the decision thresholds. If we assume high SNR for our received signal and thus $T_{\text{symbol}}A^2|h_i|^2 \gg T_{\text{symbol}}N_w$, we can say that

$$\mu_i \sim T_{\text{symbol}}A^2|h_i|^2 \quad \sigma_i^2 \sim 2N_wT_{\text{symbol}}\mu_i. \quad (17)$$

Using the above, the threshold of (15) can be simplified as

$$t_{01} \approx \frac{\sigma_1\mu_0 + \sigma_0\mu_1}{\sigma_1 + \sigma_0}. \quad (18)$$

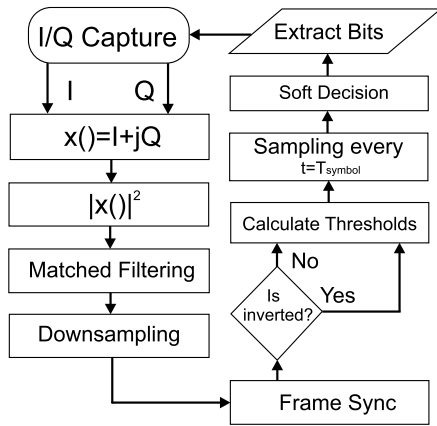


Fig. 9. Flowchart of the receiver algorithm implemented in MATLAB software.

The other two thresholds can be approximated as

$$t_{12} \approx \frac{\sigma_2 \mu_1 + \sigma_1 \mu_2}{\sigma_1 + \sigma_2} \quad t_{23} \approx \frac{\sigma_3 \mu_2 + \sigma_2 \mu_3}{\sigma_2 + \sigma_3}. \quad (19)$$

Having the three thresholds, we can take the decision and ML method performs independent detection of the four double-bit symbols according to decision areas of Fig. 7. The detection method is explained in the following.

- 1) Decide X_0 from U_0 , if $U < t_{01}$.
- 2) Decide X_1 from U_1 , if $t_{01} < U < t_{12}$.
- 3) Decide X_2 from U_2 , if $t_{12} < U < t_{23}$.
- 4) Decide X_3 from U_3 , if $t_{23} > U$.

B. Low Cost SDR

In this paper, the low cost (RTL SDR) [32] was used as receiver. It costs only 23 GBP from an Amazon supplier and it was connected with a telescopic monopole antenna for FM signals reception. The gain of the monopole is 2.15 dBi from 5 to 300 MHz. The receiver has a noise figure of around 3.5 dB and the sampling rate was fixed at 1 MSps for this work. At 98.5 MHz, the sensitivity of the receiver was estimated at -129 dBm [33] and this makes it suitable for our low cost application. The USB dongle provides real (I) and imaginary (Q) samples of the baseband signal to the GNU-radio framework. A Linux computer is required and the GNU-radio supplies the MATLAB software with samples through a first-in first-out (FIFO) buffer for real-time digital signal processing. GNU-radio pushes the data to the FIFO and MATLAB reads that data for further processing.

C. Receiver Algorithm

A modified version of previous algorithm in [18] was used for our real-time receiver algorithm. The flowchart of the 4-PAM receiver is shown in Fig. 9. The algorithm captures data in a specific time window equal with $3 \times$ packet duration and packet duration = $14 * T_{\text{symbol}}$. The baseband received signal can be expressed as

$$y[k] = y(kT_s + \tau_{TR}) = h x_r[k] + n[k] = I[k] + j Q[k] \quad (20)$$

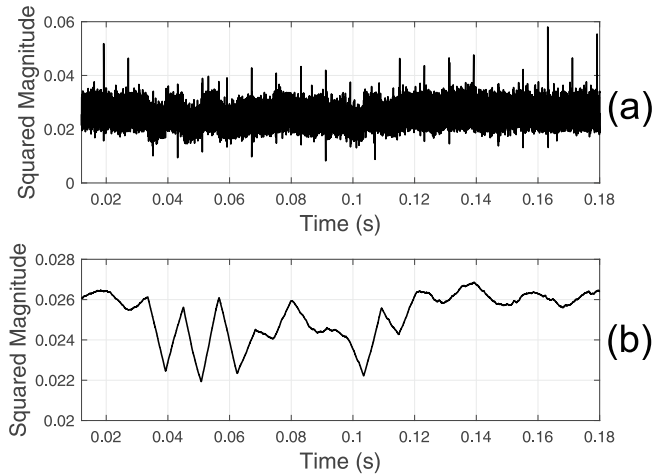


Fig. 10. Received packet signal. (a) Signal after squared absolute operation. (b) Signal after matched filtering for $T_{\text{symbol}} = 5.4$ ms.

with $n[k] = n(kT_s)$, $n[k] \sim \mathcal{N}(0, \sigma_n^2)$, and T_s the sampling period. The noise element can be defined as dc component added to our useful signal $h x_r[k]$. The $y[k]$ also includes the modulated useful information and a component based on the FM message. The absolute squared value of $y[k]$ was taken and a matched filtering was utilized to maximize the SNR. The $|y[k]|^2$ signal is CFO corrected as it is explained in [18]. The matched filter is a square pulse signal with T_{symbol} duration and acts as a low-pass filter that removes out-of-band signals. Fig. 10(a) shows an example of a received packet in time domain after the absolute square operation. The packet after the low-pass filtering is depicted in Fig. 10(b). The packet was captured using a real FM station in an indoor demo as it is explained in Section VI. It can be observed that the packet also includes spurious/noise signals from the building environment.

Following the same steps of [18], a downsampling operation by a factor of 10 was applied in order to reduce the computational complexity of the following steps without compromising the detection quality. Proper decoding requires locating where the frame starts and this step is called frame synchronization. Cross correlation was used for the synchronization with a known preamble sequence 10-00-10-00-10-01-11. As it is observed, the preamble includes all the symbols at least once and in this paper, it is used also for training. In particular, the group of training symbols is send prior to the useful data symbols and they are useful for calculation of the thresholds. More specifically, it consists of seven symbols and the last four of them are used to estimate the μ_i and σ_i of each symbol and thus the three thresholds. During synchronization, it is also detected if the signal is an inverted waveform or not. An inverted waveform (Fig. 10) results due to the multipath channel characteristics and the high level of the signal has become low and vice versa. This is detected through the comparison of the detected preamble bits with our a priori known preamble and the inverse known preamble [34]. The correlation operation that returns the maximum result, indicates where the packet starts and if it is inverted or not.

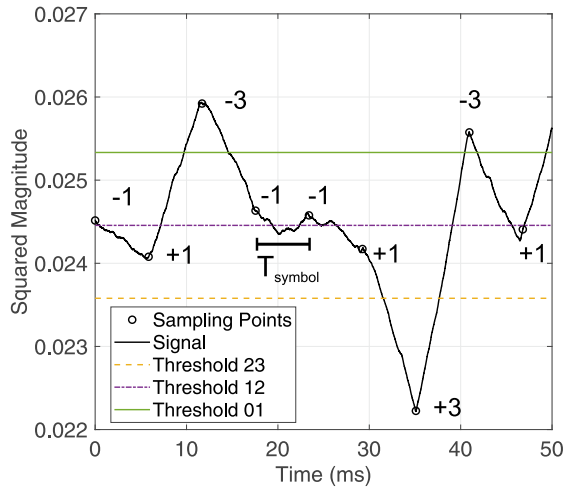


Fig. 11. Received packet without the preamble after matched filtering. The respective symbols can be decided using three thresholds.

The inversion is position dependent and this information is required for the next step.

Three amplitude thresholds are calculated using the theoretical formulations of (18) and (19). For each packet coming at the receiver, it is necessary to calculate different thresholds and thus different μ_i , σ_i values. In Fig. 11, the estimated thresholds for the signal of Fig. 10 are depicted. The thresholds are inverted because our initial signal was inverted.

Next, the algorithm quantizes the received signal based on the three thresholds. Samples every T_{symbol} are taken and compared with threshold(s) to determine the recovered data symbols. A transmitted symbol is determined if the sample corresponds to its specific symbol region. Fig. 11 depicts the useful signal of Fig. 10 without the preamble bits and a specific symbol/region corresponds to a received sample for a given T_{symbol} . Finally, a quantizer makes the decisions that are then decoded back from symbols to the bits of the message. In Fig. 11, it can be observed that the distances between symbols are not equal or maximized instead of the Γ_i in Fig. 6. In the RF front-end design, we assumed that the antenna is matched to 50Ω and we used a commercial antenna afterward. The monopole antenna was not well matched thus the GND plane of our RF front-end was small, and this leads to a discrepancy from the desired reflection coefficients. As a result, there is a corresponding reduction in the distance between the symbols and thus performance degradation. As part of future work, we will optimize the bias points taking into account the measured antenna impedance values.

VI. MEASUREMENT RESULTS

In order to evaluate telecommunication measurements for our system, the proof-of-concept tag prototype was programmed to produce a fixed packet bit-stream at the DAC output. The symbol representation of bit sequence was described above and it is depicted in Fig. 8. Fig. 8 shows an oscilloscope measurement and the four voltage levels of the transmitted symbols that are used to drive the transistor. The T_{symbol} was fixed at 5.8 ms, and thus the bit rate is calculated at 345 b/s.

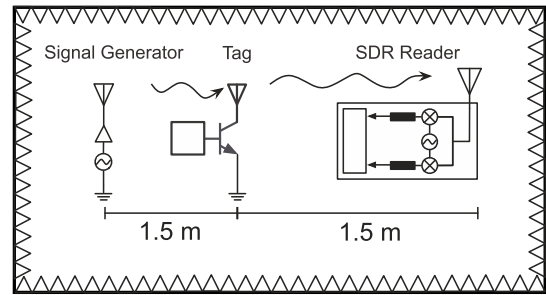


Fig. 12. Schematic of the experimental setup in the anechoic chamber. The transmitter-to-tag distance and the tag-to-reader distance were 1.5 m.

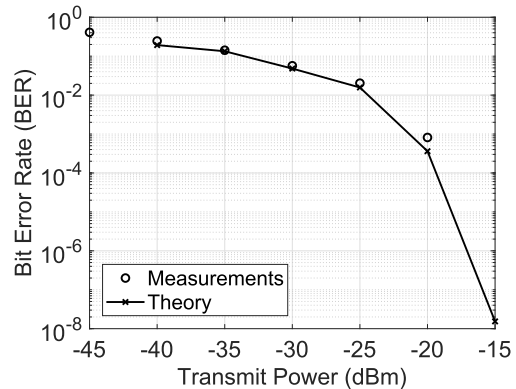


Fig. 13. Experimental bit error rate (BER) versus the transmitted power at the generator. The bit rate was 345 b/s and the distances transmitter-to-tag, tag-to-reader were 1.5 m.

It can be observed that a small variation between the gate voltages corresponding to the states -1 and $+1$ occurs. This variation does not correspond to small variation in Γ_i but leads to the maximum distance between Γ_1 and Γ_2 as it is shown in Fig. 6. This is due to the nonlinear relationship between the transistor gate voltage and the corresponding Γ_i .

To test the performance of the backscatter communication link, we first demonstrated our system in a controlled environment (anechoic chamber). The same setup, lab equipment and configuration with [18] was used. The RF front-end antenna was placed 1.5 m away from the receiver antenna while the FM generator antenna was 1.5 m way from the tag. The generator and the reader use commercial passive FM antennas with gain 2.15 dBi. For our deployment, we used the bistatic architecture where the illuminating CW emitter and the receiver of the reflected signals are distinct units, located at different positions. The bistatic topology is shown in Fig. 12 and the signal generator was set at 98.5 MHz. Different transmit power levels were recoded at the generator while the tag was set to send the fixed packet continuously. At the receiver, the bandwidth around the carrier frequency was fixed at 1 MHz. In order to compute the bit error rate (BER), 1200 packets of data were collected for a varying transmit power from -45 to -20 dBm. Each packet contains 28 bits and thus the transmitted bits were 33 600. The resulting BER versus the transmit power is shown in Fig. 13 and the minimum BER value at -20 dBm was measured to be 8.16×10^{-4} .

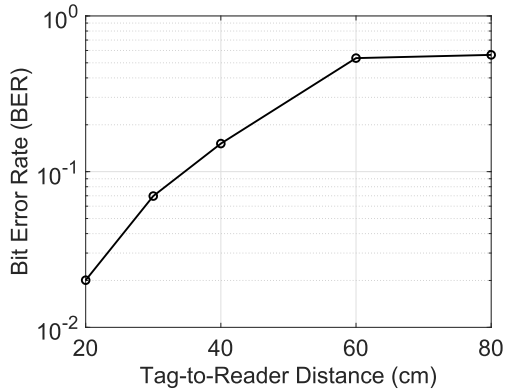


Fig. 14. Measured bit error rate (BER) versus the tag-to-reader distance. An FM station 34 km away was used and the communication bit rate was 345 b/s.

In [18], we use two-ASK modulation with FM0 encoding and was showed that BER approached 2.5×10^{-3} when the transmit power was -30 dBm. As expected, the BER increased as the power at the generator decreases thus the reader cannot decode successfully the packets. In Fig. 13, the theoretical BER results are also depicted along with the measurements.

For the theoretical calculations of BER (P_b), the formula of (11) is used with the four corresponding Q functions of (12). Using a capture of 100 packets, we calculated the μ_i value and the σ_i value of each symbol and thus the thresholds. In order to achieve accurate results, we used all the symbols of the packet and not only from the preamble. A good agreement between simulation and measurement results can be observed. Theoretical results were performed for transmitted power up to -15 dBm where the BER approached 10^{-8} . For 10^{-8} BER we need $3 \times 10^{+8}$ bits for a confidence level of 0.95 [18] and in the measurements we used only 33 600 transmitted bits.

The system was also tested indoors using the most powerful FM station that was measured in the building [18]. It corresponds to the BBC 95.8 MHz station which is located around 34.65 km away from the experimental setup. The radiated power of the FM station was 250 KW and the power of the received FM signal next to the tag antenna and was measured with a spectrum analyzer at -40 dBm. The BER was measured for different tag-to-reader distances, and the BER results are shown in Fig. 14 for a fixed bit rate of 345 b/s.

For power consumption comparison and validation purposes, two-ASK binary modulation with FM0 encoding [18] was designed on this proof-of-concept tag. The proposed MCU was used without the DAC, thus binary modulation requires only a digital output pin in order to control the transistor. For the two ASK and using the clock of 32 kHz, the minimum T_{symbol} achieved was 3.4 ms and it corresponds to a bit rate of 147 b/s. Table II presents the average power consumption results for two ASK and 4-PAM in addition to corresponding bit rates. In binary modulation, the average power dissipation was measured at $6.48 \mu\text{W}$ when the ADC was OFF and $396 \mu\text{W}$ when the ADC was activated. The ADC is used for sensing and it is turned OFF exactly after the data collection in order to reduce the average power consumption. Using the

TABLE II
TAG POWER CONSUMPTION CHARACTERISTICS

Operation Mode	μW	Bit rate (kbps)
Sleep: (no DAC, no ADC)	1.08	0
Active: 2-ASK (no DAC, no ADC)	6.48	0.147
Active: 2-ASK (no DAC, ADC)	396	0.147
Active: 4-PAM (DAC, no ADC)	27	0.345
Active: 4-PAM (DAC, ADC)	432	0.345
Active: 4-PAM (DAC, no ADC)	283	10.2
Active: 4-PAM (DAC, ADC)	501	10.2

high-order modulation, the 4-PAM was measured at $27 \mu\text{W}$ with the ADC disabled and $432 \mu\text{W}$ with ADC turned ON. The proposed tag was programmed in a higher bit rate of 10.2 kb/s only for power measurements purpose and the power consumption was measured at $501 \mu\text{W}$ when the ADC was turned ON and $501 \mu\text{W}$ when the ADC was OFF. An increment of power consumption of the tag plus the modulator (RF transistor) is observed for 4-PAM when is programmed at a higher bit rate. There is also a tradeoff between the bit rate and the power consumption across the two modulation schemes. The bit rate is almost duplicated but the consumption is not, due to the nonlinear behaviour of the DAC component.

VII. DISCUSSION

The dc power consumption reported in this paper compared with all the similar referenced works so far, are summarized in Table III. The table presents all the designs that include hardware implementation and use only high-order modulation over a CW/ambient signal in order to communicate. Our tag has been measured at low bit rate using ambient FM signals for communication and ensure fair comparison with the other works. As shown, this works represents the lowest power consumption ambient backscatter hardware prototype implementation with high-order modulation, reported to date. The energy per bit was calculated at 78 nJ/bit for 345 b/s and 27.7 nJ/bit for 10.2 kb/s including the energy consumption of the modulator (RF transistor). In [7], the static dc power consumption of the modulator, excluding the power consumption of the microcontroller, was 115 nW corresponding to a data rate of 400 kb/s. The tag was fixed at 2.92 m away from the transmitter antenna with effective isotropic radiated power (EIRP) $+38.4$ dBm. In their prototype tag, an MSP430 microcontroller was consuming an additional 3–6 mW when generating the data. A CR2032 3 V lithium coin cell battery was used as a power source for the device. In [9], the semipassive device was using a CR2032 3 V coin cell battery for dc power and it was capable of transmitting 96 Mb/s with the modulator consuming 1.49 mW (15.5 pJ/bit). Using a transmitter with $+23$ dBm EIRP, the backscatter data link had a measured operating distance of 1.24 m in a typical indoor environment. Thomas *et al.* [7] and Thomas and Reynolds [9] were utilizing 4-QAM and 16-QAM, respectively, on an UHF CW signal. In [10], the value of energy spent in the 16-QAM modulator was 16.7 pJ/bit for a data rate of 60 Mb/s and the average power consumption was estimated at 1 mW. Shirane *et al.* [11] presents a 113 μW 32-QAM transmitter employing the backscattering technique

TABLE III
HIGH-ORDER MODULATION BACKSCATTER DESIGNS

Work	Modulation	Backscatter Signal	Power	Part	Bit rate	Energy/bit	Range (m)
This work	4-PAM	Ambient FM	27 μ W (Measurement)	Tag+Modulator	345 bps	78.2 nJ/bit	1
This work	4-PAM	Ambient FM	501 μ W (Measurement)	Tag+Modulator	10.2 Kbps	27.7 nJ/bit	-
[7]	4-QAM	UHF CW	115 nW+6mW (Measurement)	Tag+Modulator	400 kbps	15 nJ/bit	2.92
[9]	16-QAM	UHF CW	1.49 mW (Measurement)	Modulator	96 Mbps	15.5 pJ/bit	1.24
[10]	16-QAM	UHF CW	1 mW (Measurement)	Modulator	60 Mbps	6.7 pJ/bit	-
[11]	32-QAM	5.8 GHz CW	113 μ W (Simulation)	Tag+Modulator	2.5 Mbps	49.1 pJ/bit	-
[15]	4-PSK	UHF TV	-	Tag+Modulator	20 kbps	-	0.7
[16]	4-QAM	Cellular & Wi-Fi	27 nW (Simulation)	Modulator	500 kbps	0.054 pJ/bit	-
[17]	4-FSK	Ambient FM	11.07 μ W (Simulation)	Tag+Modulator	3.2 kbps	3.46 nJ/bit	4.8

for the transmitting part. In [15], a 4-PSK hardware prototype link was implemented using ambient signals. Two tags can communicate with information rate of 20 kb/s over a distance of 0.7 m. An RF source was setup to transmit the single tone at 539 MHz with power 10 dBm. In [16], a system capable of modulating the ambient signals was designed for two different ambient sources (cellular and Wi-Fi signals) with 4-QAM high-order modulation. Considering a data rate of 500 kb/s, the power consumption of the modulator was 27 nW with 0.054 pJ energy per bit. The designs of [10] and [16] were tested using a signal generator to generate the transmitter signals and an arbitrary waveform generator to generate the voltage levels at the gate of each transistor. A coupler was used to measure the reflected signal from the circuit, by a VNA. Finally, in [17], the ambient signals were used for communication and for their tag, they simulated an integrated circuit that backscatters audio signals, and showed that it consumes 11.07 μ W at 3.2 kb/s bit rate. For testing their 4-FSK modulator prototype, they used an arbitrary waveform generator. An USRP transmitter was setup to broadcast mono and stereo audio signals with power up to -60 dBm. For transmit power -60 dBm at 1.6 and 3.2 kb/s, the BER was low at distances (tag-to-reader) as high as 4.8 m. Further, at 1.6 kb/s, the BERs were still low up to 0.9 m and 1.82 m at -60 and -50 dBm, respectively.

An alternative solution for our RF front-end is the use of four lumped impedances instead of one transistor. For example, the modulator in [7] and [15] includes a 4-to-1 Mux (a SP4T CMOS RF switch) to modulate the circuit impedance between four impedance states. It can be thought of as an “impedance DAC” that converts a 2-bit digital input to a specified modulating impedance. The multistate RF switch based modulator is power efficient as the DAC solution, though it tradeoff the board area and the more complex implementation. In case of an IC implementation it is required bigger die area because four switched impedances are required to implement four-ary modulation. The solution of a simple impedance transistor and a DAC seems to be a promising solution with similar power consumption but reduced die area.

A future challenge for this work is to employ communication measurements (BER) for the 2-PAM using this tag and compare them with the existing high-order modulation results. Finally, a new compact RF front-end could be designed and optimized together with a coil FM antenna on the same substrate. At the receiver part, we focus to transmit our useful signals to smartphones using FM backscatter communication.

The TV signals are an alternative solution for the ambient source due to their shorter wavelength which means small antennas. Since our application will take advantage on the fact that smartphones have FM receivers, the TV signals do not fulfil our requirements.

The tag that is proposed in this work is semipassive since it uses a super capacitor for power supply. With the utilization of the bistatic topology and semipassive tags that communicate with a low bit rate, it is possible to implement a wireless sensor network, comprising the proposed low-cost sensor/tags. The application shown in Fig. 1 require that multiple tags could be supported. In that scenario, multiple tags could communicate with only one reader using a time-division-multiple-access scheme. Each tag could be programmed to work in a duty cycle operation in order to minimize the average power consumption. Each tag will be active only for a desired minimum period of time (i.e., send two packets) and in “sleep” mode for most of the time where the power consumption is only 1.08 μ W. The receiver could sent a pure CW signal in order to wake up the nearby tags from the “sleep” mode. The tags could send their information in random intervals in order to avoid a possible signal collision.

VIII. CONCLUSION

In this paper, we designed and integrated an ultra-low-power sensor node/tag with ambient FM backscatter and high-order modulation capabilities. The tag can read up to four sensors and modulate the information using 4-PAM modulation instead of the binary 2-PAM. The transmitted bit rate is duplicated and the tag uses the ambient FM signals in order to send the data to a low-cost SDR reader. A real-time algorithm was implemented in order to read the reflected signals and communication was demonstrated experimentally indoors. The tag does not require batteries and was supplied with a small solar panel consuming only 27 μ W. This high-order modulation approach is the first demonstration of backscatter 4-PAM modulation on ambient FM signals. It also paves the way for practical deployments for short range, ultra-low-power backscatter sensors such as wearable body area sensors.

ACKNOWLEDGMENT

Authors S. N. Daskalakis, G. Goussetis, and A. Georgiadis would like to thank the Lloyd’s Register Foundation and International Consortium in Nanotechnology. The authors would like to thank all members of the Microwaves and

Antenna Engineering Research Group, Heriot-Watt University, Edinburgh, U.K., for their help in various steps throughout this paper .

REFERENCES

- [1] EPC Global. (2015). *Specification for RFID Air Interface Protocol for Communications at 860 MHz-960 MHz, Version 2.0.1*. [Online]. Available: https://www.gs1.org/sites/default/files/docs/epc/Gen2_Protocol_Standard.pdf
- [2] S. N. Daskalakis, S. D. Assimonis, E. Kampianakis, and A. Bletsas, "Soil moisture wireless sensing with analog scatter radio, low power, ultra-low cost and extended communication ranges," in *Proc. IEEE SENSORS*, Nov. 2014, pp. 122–125.
- [3] S. N. Daskalakis, G. Goussetis, S. D. Assimonis, M. M. Tentzeris, and A. Georgiadis, "A μ W backscatter-morse-leaf sensor for low-power agricultural wireless sensor networks," *IEEE Sensors J.*, vol. 18, no. 19, pp. 7889–7898, Oct. 2018.
- [4] A. P. Sample, D. J. Yeager, P. S. Powlidge, A. V. Mamishev, and J. R. Smith, "Design of an RFID-based battery-free programmable sensing platform," *IEEE Trans. Instrum. Meas.*, vol. 57, no. 11, pp. 2608–2615, Nov. 2008.
- [5] E. Kampianakis, A. Sharma, J. Arenas, and M. S. Reynold, "A dual-band wireless power transfer and backscatter communication approach for real-time neural/EMG data acquisition," *IEEE J. Radio Freq. Identificat.*, vol. 1, no. 1, pp. 100–107, Mar. 2017.
- [6] S. Thomas and M. S. Reynolds, "QAM backscatter for passive UHF RFID tags," in *Proc. IEEE Int. Conf. RFID*, Orlando, FL, USA, Apr. 2010, pp. 210–214.
- [7] S. J. Thomas, E. Wheeler, J. Teizer, and M. S. Reynolds, "Quadrature amplitude modulated backscatter in passive and semipassive UHF RFID systems," *IEEE Trans. Microw. Theory Techn.*, vol. 60, no. 4, pp. 1175–1182, Apr. 2012.
- [8] J. Kimionis, A. Georgiadis, and M. M. Tentzeris, "Millimeter-wave backscatter: A quantum leap for gigabit communication, RF sensing, and wearables," in *IEEE MTT-S Int. Microw. Symp. Dig.*, Honolulu, HI, USA, Jun. 2017, pp. 812–815.
- [9] S. J. Thomas and M. S. Reynolds, "A 96 Mbit/sec, 15.5 pJ/bit 16-QAM modulator for UHF backscatter communication," in *Proc. IEEE Int. Conf. RFID*, Orlando, FL, USA, Apr. 2012, pp. 185–190.
- [10] R. Correia, A. Boaventura, and N. B. Carvalho, "Quadrature amplitude backscatter modulator for passive wireless sensors in IoT applications," *IEEE Trans. Microw. Theory Techn.*, vol. 65, no. 4, pp. 1103–1110, Apr. 2017.
- [11] A. Shirane *et al.*, "A 5.8 GHz RF-powered transceiver with a 113 μ W 32-QAM transmitter employing the IF-based quadrature backscattering technique," in *IEEE Int. Solid-State Circuits Conf. (ISSCC) Dig. Tech. Papers*, San Francisco, CA, USA, 2015, pp. 1–3.
- [12] C. Boyer and S. Roy, "Backscatter communication and RFID: Coding, energy, and MIMO analysis," *IEEE Trans. Commun.*, vol. 62, no. 3, pp. 770–785, Mar. 2014.
- [13] V. Liu, A. Parks, V. Talla, S. Gollakota, D. Wetherall, and J. R. Smith, "Ambient backscatter: Wireless communication out of thin air," *ACM SIGCOMM*, vol. 43, no. 4, pp. 39–50, Aug. 2013.
- [14] N. Van Huynh, D. T. Hoang, X. Lu, D. Niyato, P. Wang, and D. I. Kim. (Dec. 2017). "Ambient backscatter communications: A contemporary survey." [Online]. Available: <https://arxiv.org/abs/1712.04804>
- [15] J. Qian, A. N. Parks, J. R. Smith, F. Gao, and S. Jin, "IoT communications with M-PSK modulated ambient backscatter: Algorithm, analysis, and implementation," *IEEE Internet Things J.*, Jul. 2018.
- [16] R. Correia and N. B. Carvalho, "Dual-band high order modulation ambient backscatter," in *IEEE MTT-S Int. Microw. Symp. Dig.*, Philadelphia, PA, USA, Jun. 2018, pp. 270–273.
- [17] A. Wang, V. Iyer, V. Talla, J. R. Smith, and S. Gollakota, "FM backscatter: Enabling connected cities and smart fabrics," in *Proc. 14th USENIX Symp. Netw. Syst. Design Implement. (NSDI'17)*, Boston, MA, Mar. 2017, pp. 243–258.
- [18] S. N. Daskalakis, J. Kimionis, A. Collado, G. Goussetis, M. M. Tentzeris, and A. Georgiadis, "Ambient backscatterers using FM broadcasting for low cost and low power wireless applications," *IEEE Trans. Microw. Theory Techn.*, vol. 65, no. 12, pp. 5251–5262, Dec. 2017.
- [19] S. N. Daskalakis, R. Correia, G. Goussetis, M. M. Tentzeris, N. B. Carvalho, and A. Georgiadis, "Spectrally efficient 4-PAM ambient FM backscattering for wireless sensing and RFID applications," in *IEEE MTT-S Int. Microw. Symp. Dig.*, Philadelphia, PA, USA, Jun. 2018, pp. 266–269.
- [20] Microchip Technology. (2014). *PIC16LF1459 USB Microcontroller With Extreme Low-Power Technology*. [Online]. Available: <http://www.microchip.com/downloads/en/DeviceDoc/40001639B.pdf>
- [21] PowerFilm. (2009). *SP3-37 Flexible Solar Panel 3V @ 22mA*. [Online]. Available: <https://goo.gl/q5ECXh>
- [22] Uorex Semiconductor. (2012). *XC6504 0.6 μ A Ultra Low Power Consumption Voltage Regulator*. [Online]. Available: <https://www.torexsemi.com/file/xc6504/XC6504.pdf>
- [23] S. D. Assimonis, S.-N. Daskalakis, and A. Bletsas, "Efficient RF harvesting for low-power input with low-cost lossy substrate rectenna grid," in *Proc. IEEE RFID Technol. Appl. Conf. (RFID-TA)*, Tampere, Finland, Sep. 2014, pp. 1–6.
- [24] K. Niotaki, A. Collado, A. Georgiadis, S. Kim, and M. M. Tentzeris, "Solar/electromagnetic energy harvesting and wireless power transmission," *Proc. IEEE*, vol. 102, no. 11, pp. 1712–1722, Nov. 2014.
- [25] X. Gu, S. Hemour, L. Guo, and K. Wu, "Integrated cooperative ambient power harvester collecting ubiquitous radio frequency and kinetic energy," *IEEE Trans. Microw. Theory Techn.*, vol. 66, no. 9, pp. 4178–4190, Sep. 2018.
- [26] Broadcom. (2006). *ATF-52189 High Linearity Mode Enhancement Pseudomorphic HEMT FET Transistor, product manual*. [Online]. Available: <https://www.broadcom.com/products/wireless/transistors/fet/atf-52189>
- [27] A. Bletsas, A. G. Dimitriou, and J. N. Sahalos, "Improving backscatter radio tag efficiency," *IEEE Trans. Microw. Theory Techn.*, vol. 58, no. 6, pp. 1502–1509, Jun. 2010.
- [28] C. R. Johnson, Jr., W. A. Sethares, and A. G. Klein, *Software Receiver Design: Build your Own Digital Communication System in Five Easy Steps*. Cambridge, U.K.: Cambridge Univ. Press, 2011.
- [29] J. G. Proakis and M. Salehi, *Digital Communications*, 5th ed. New York, NY, USA: McGraw-Hill, 2008.
- [30] J. Qian, F. Gao, G. Wang, S. Jin, and H. Zhu, "Noncoherent detections for ambient backscatter system," *IEEE Trans. Wireless Commun.*, vol. 16, no. 3, pp. 1412–1422, Mar. 2017.
- [31] P. N. Alevizos, Y. Fountzoulas, G. N. Karystinos, and A. Bletsas, "Log-linear-complexity GLRT-optimal noncoherent sequence detection for orthogonal and RFID-oriented modulations," *IEEE Trans. Commun.*, vol. 64, no. 4, pp. 1600–1612, Apr. 2016.
- [32] NooElec. (2017). *NESDR SMARt Bundle-Premium RTL-SDR*. [Online]. Available: <http://www.nooelec.com/store/nesdr-smart.html>
- [33] B. Clarke and K. Kreitzer, "Maximizing the dynamic range of software-defined radio," Analog Devices, Norwood, MA, USA, Tech. Rep. MS-2735, 2014, pp. 1–4.
- [34] M. Bamiedakis-Pananos, "Synchronization and detection for Gen2 RFID signals," M.S. thesis, School Elect. Comput. Eng., Tech. Univ. Crete, Chania, Greece, 2015.



Spyridon Nektarios Daskalakis (S'12) was born in Heraklion, Greece, in 1991. He received the Engineering Diploma and M.Sc. degrees in electrical and computer engineering from the Technical University of Crete, Chania, Greece, in 2014 and 2016, respectively. He is currently pursuing the Ph.D. degree at the School of Engineering and Physical Sciences, Heriot-Watt University, Edinburgh, U.K.

His current research interests include low-power, low-cost wireless sensor networks, energy harvesting, backscatter radio communication, batteryless

sensors, low cost software-defined radio, environmental sensing, and RF energy harvesting.

Mr. Daskalakis has been a member of the IEEE Microwave Theory and Techniques Society, the IEEE Council on RFID, and the IEEE Sensors Council. He was a recipient of the Fellowship Award by the Clinton Global Initiative University 2014 (USA), the Onassis Foundation (Graduate Studies 2015/2016 Scholarship), the Lloyds Register Foundation, the International Consortium in Nanotechnology, the two short-term scientific mission grants from COST Action IC1301 WiPE of the School of Electrical and Computer Engineering, Georgia Institute of Technology, Atlanta, GA, USA, in 2016, and the Centre Tecnològic de Telecomunicacions de Catalunya, Barcelona, Spain, in 2015.



Ricardo Correia (GS'15) received the M.Sc. degree in electronics and telecommunications engineering from the University of Aveiro, Aveiro, Portugal, in 2009, where he is currently pursuing the Ph.D. degree in electrical engineering.

He was an Automation and Electrical Engineer and a Researcher in embedded systems and signal processing. He is currently a Researcher with the Institute of Telecommunications, University of Aveiro. His current research interests include wireless power transfer, energy harvesting, wireless passive sensors for space applications, and low-power communications.

Mr. Correia is a member of the IEEE Microwave Theory and Techniques Society. He is also a Reviewer for the *IET Microwaves, Antennas and Propagation*, *Wireless Power Transfer Journal* and the IEEE TRANSACTIONS ON MICROWAVE THEORY AND TECHNIQUES. He was a recipient of the 2016 URSI/ANACOM Prize awarded by the URSI Portuguese Section and Portuguese National Authority of Communications.



George Goussetis (S'99–M'02–SM'12) received the Diploma degree in electrical and computer engineering from the National Technical University of Athens, Athens, Greece, in 1998, and the Ph.D. degree from the University of Westminster, London, U.K., in 2002, and the B.Sc. degree (First Class) in physics from University College London, London, U.K.

In 1998, he joined the Space Engineering, Rome, Italy, as an RF Engineer and the Wireless Communications Research Group, University of Westminster, as a Research Assistant in 1999. From 2002 to 2006, he was a Senior Research Fellow with Loughborough University, Loughborough, U.K. From 2006 to 2009, he was a Lecturer (Assistant Professor) with Heriot-Watt University, Edinburgh, U.K., and a Reader (Associate Professor) with Queens University Belfast, U.K., from 2009 to 2013. In 2013, he joined Heriot-Watt University as a Reader, where he became a Professor in 2014, and currently directs the Institute of Sensors Signals and Systems. He has authored or co-authored over 500 peer-reviewed papers, 5 book chapters, 1 book, and 4 patents. His current research interests include microwave and antenna components and subsystems.

Dr. Goussetis was a co-recipient of the 2011 European Space Agency Young Engineer of the Year Prize, the 2011 EuCAP Best Student Paper Prize, the 2012 EuCAP Best Antenna Theory Paper Prize, and the 2016 Bell Labs Prize. He has served as an Associate Editor of IEEE ANTENNAS AND WIRELESS PROPAGATION LETTERS. He has held a Research Fellowship from the Onassis Foundation in 2001, the U.K. Royal Academy of Engineering between 2006 and 2011, and the European Marie-Curie Experienced Researcher Fellowship from 2011 to 2012 and from 2014 to 2017.



Manos M. Tentzeris (S'89–M'98–SM'03–F'10) received the Diploma degree (*magna cum laude*) in electrical and computer engineering from the National Technical University of Athens, Athens, Greece, and the M.S. and Ph.D. degrees in electrical engineering and computer science from the University of Michigan, Ann Arbor, MI, USA.

He is currently a Ken Byers Professor in flexible electronics with the School of Electrical and Computer Engineering, Georgia Institute of Technology, Atlanta, GA, USA. He has authored over 650 papers in refereed journals and conference proceedings, 5 books, and 25 book chapters. He has helped develop academic programs in 3-D/inkjet-printed RF electronics and modules, flexible electronics, origami and morphing electromagnetics, highly integrated/multilayer packaging for RF and wireless applications using ceramic and organic flexible materials, paper-based RFID's and sensors, wireless sensors and biosensors, wearable electronics, "Green" electronics, energy harvesting and wireless power transfer, nanotechnology applications in RF, microwave MEM's, SOP-integrated (UWB, multiband, millimeter wave, and conformal) antennas, and heads the ATHENA research group (20 researchers). He has served as the Head of the ECE Electromagnetics Technical Interest Group, Institute of Technology, as the Georgia Electronic Design Center Associate Director for RFID/Sensors research and as the Georgia Tech NSF-Packaging Research Center Associate Director for RF Research and the RF Alliance Leader. He was a Visiting Professor with the Technical University of Munich, Germany in 2002, a Visiting Professor with GTRI-Ireland in Athlone, Ireland, in 2009, and a Visiting Professor with LAAS-CNRS, Toulouse, France, in 2010. He has given more than 100 invited talks to various universities and companies all over the world.

Dr. Tentzeris was a recipient or co-recipient of the 2017 Georgia Institute of Technology Outstanding Achievement in Research Program Development Award, the 2016 Bell Labs Award Competition 3rd Prize, the 2015 IET Microwaves, Antennas and Propagation Premium Award, the 2014 Georgia Institute of Technology ECE Distinguished Faculty Achievement Award, the 2014 IEEE RFID-TA Best Student Paper Award, the 2013 IET Microwaves, Antennas and Propagation Premium Award, the 2012 FiDiPro Award in Finland, the iCMG Architecture Award of Excellence, the 2010 IEEE Antennas and Propagation Society Piergiorgio L. E. Uslenghi Letters Prize Paper Award, the 2011 International Workshop on Structural Health Monitoring Best Student Paper Award, the 2010 Georgia Institute of Technology Senior Faculty Outstanding Undergraduate Research Mentor Award, the 2009 IEEE Transactions on Components and Packaging Technologies Best Paper Award, the 2009 E. T. S. Walton Award from the Irish Science Foundation, the 2007 IEEE APS Symposium Best Student Paper Award, the 2007 IEEE IMS Third Best Student Paper Award, the 2007 ISAP 2007 Poster Presentation Award, the 2006 IEEE MTT-S Outstanding Young Engineer Award, the 2006 Asia-Pacific Microwave Conference Award, the 2004 IEEE TRANSACTIONS ON ADVANCED PACKAGING Commendable Paper Award, the 2003 NASA Godfrey "Art" Anzic Collaborative Distinguished Publication Award, the 2003 IBC International Educator of the Year Award, the 2003 IEEE CPMT Outstanding Young Engineer Award, the 2002 International Conference on Microwave and Millimeter-Wave Technology Best Paper Award (Beijing, China), the 2002 Georgia Institute of Technology-ECE Outstanding Junior Faculty Award, the 2001 ACES Conference Best Paper Award and the 2000 NSF CAREER Award, and the 1997 Best Paper Award of the International Hybrid Microelectronics and Packaging Society. He was the TPC Chair for IEEE IMS 2008 Symposium and the Chair of the 2005 IEEE CEM-TD Workshop. He is the Vice-Chair of the RF Technical Committee (TC16) of the IEEE CPMT Society. He is the founder and the Chair of the RFID Technical Committee (TC24) of the IEEE MTT-S and the Secretary/Treasurer of the IEEE C-RFID. He is an Associate Editor of the IEEE TRANSACTIONS ON MICROWAVE THEORY AND TECHNIQUES, the IEEE TRANSACTIONS ON ADVANCED PACKAGING and *International Journal on Antennas and Propagation*. He is a member of URSI-Commission D, the MTT-15 Committee, and the Technical Chamber of Greece. He is an Associate Member of EuMA and a Fellow of the Electromagnetic Academy. He served as one of the IEEE MTT-S Distinguished Microwave Lecturers from 2010 to 2012 and is one of the IEEE CRFID Distinguished Lecturers.



Nuno Borges Carvalho (S'97–M'00–SM'05–F'15) was born in Luanda, Angola, in 1972. He received the diploma and doctoral degrees in electronics and telecommunications engineering from the University of Aveiro, Aveiro, Portugal, in 1995 and 2000, respectively.

He is currently a Full Professor and a Senior Research Scientist with the Institute of Telecommunications, University of Aveiro. He co-authored *Intermodulation in Microwave and Wireless Circuits* (Artech House, 2003), *Microwave and Wireless Measurement Techniques* (Cambridge Univ. Press, 2013), and *White Space Communication Technologies* (Cambridge Univ. Press, 2014). He has been a Reviewer and author of over 200 papers in magazines and conferences. His current research interests include software-defined radio front-end, wireless power transmission, nonlinear distortion analysis in microwave/wireless circuits and systems, measurement of nonlinear phenomena, design of dedicated radios and systems for newly emerging wireless technologies. He is the co-inventor of six patents.

Dr. Borges Carvalho is a member of the IEEE MTT AdCom, the Chair of the IEEE MTT-20 Technical Committee, and the Past-Chair of the IEEE Portuguese Section and MTT-11 and also belong to the Technical Committees, MTT-24, and MTT-26. He is also the Vice-Chair of the URSI Commission A (Metrology Group). He was a recipient of the 1995 University of Aveiro and the Portuguese Engineering Association Prize for the Best 1995 Student at the University of Aveiro, the 1998 Student Paper Competition (Third Place) of the IEEE Microwave Theory and Techniques Society International Microwave Symposium, and the 2000 IEEE Measurement Prize. He is a Distinguished Microwave Lecturer for the IEEE Microwave Theory and Techniques Society. He is the Editor-in-Chief of the *Cambridge Wireless Power Transfer Journal*, an Associate Editor of *IEEE Microwave Magazine* and a former Associate Editor of the IEEE TRANSACTIONS ON MICROWAVE THEORY AND TECHNIQUES and *IET Microwaves Antennas and Propagation Journal*.



Apostolos Georgiadis (S'94–M'02–SM'08) was born in Thessaloniki, Greece. He received the B.S. degree in physics and M.S. degree in telecommunications from the Aristotle University of Thessaloniki, Thessaloniki, Greece, in 1993 and 1996, respectively, and the Ph.D. degree in electrical engineering from the University of Massachusetts, Amherst, MA, USA, in 2002.

In 2002, he joined Global Communications Devices, North Andover, MA, USA, as a Systems Engineer, where he was involved in CMOS transceivers for wireless network applications. In 2003, he joined Bermai Inc., Minnetonka, MN, USA, as an RF/Analog Systems Architect. In 2005, he joined the University of Cantabria, Santander, Spain, as a Juan de la Cierva Fellow Researcher. In 2006, he was a Consultant for Bitwave Semiconductor, Lowell, MA, USA. He collaborated with ACORDE S.A., Santander, Spain, where he was involved in the design of integrated CMOS VCOs for ultra-wideband applications. In 2007, he joined the Technological Telecommunications Center of Catalonia (CTTC), Castelldefels, Spain, as a Senior Researcher of communications subsystems, where he was a Group Leader with the Microwave Systems and Nanotechnology Department from 2013 to 2016. In 2016, he joined Heriot-Watt University, Edinburgh, U.K., as an Associate Professor. He has authored over 180 papers in peer-reviewed

journals and international conferences. His current research interests include energy harvesting and wireless power transmission, RFID technology, active antennas and phased-array antennas, inkjet, and 3-D printed electronics, and millimeter-wave systems.

Dr. Georgiadis was a recipient of the Fulbright Scholarship for graduate studies at the University of Massachusetts, in 1996. He was the General Chair of the 2011 IEEE RFID-TA Conference and the General Co-Chair of the 2011 IEEE MTT-S IMWS on Millimeter Wave Integration Technologies. He is an EU Marie Curie Global Fellow. He is member of the IEEE MTT-S TC-24 RFID Technologies (past Chair) and a member of the IEEE MTT-S TC-26 Wireless Energy Transfer and Conversion. He was an Associate Editor of the *IET Microwaves Antennas and Propagation Journal*, IEEE MICROWAVE AND WIRELESS COMPONENTS LETTERS, and the IEEE RADIO FREQUENCY IDENTIFICATION VIRTUAL JOURNAL. He serves as an Associate Editor for the IEEE JOURNAL OF RFID and is the founder and the Editor-in-Chief of the *Wireless Power Transfer Journal* of Cambridge University Press. He is the Chair of the URSI Commission D, Electronics, and Photonics, and an AdCom member of the IEEE Council on RFID serving as the Vice President of conferences. He is a Distinguished Lecturer of the IEEE Council on RFID. In 2016, his proposal for Inkjet/3-D printed millimeter-wave systems received the Bell Labs Prize, third place among more than 250 proposals recognizing ideas that “change the game” in the field of information and communications technologies.